"RoboLase": Internet-accessible robotic laser scissors and laser tweezers microscope systems

Linda Z. Shi[1], Michael W. Berns[1, 2, 3] and Elliot Botvinick[2, 3]
[1]Department of Bioengineering, University of California, San Diego,
[2]Beckman Laser Institute, University of California, Irvine,
[3]Deparment of Biomedical Engineering, University of California, Irvine
USA[1]

1. Introduction

The advent of the internet has opened the door to remote computing, remote file sharing and remote instrumentation control. We have taken advantage of these capabilities to: (1) satisfy our need for 24-hour access to the laser-microscope, and (2) facilitate collaboration and networking with investigators from other locations around the world. The remote operation of microscope systems has been demonstrated for electron microscopes (Chumbley, et al., 2002, Hadida-Hassan, et al., 1999, Takaoka, et al., 2000, Yamada, et al., 2003), for light microscope evaluation of fixed samples (Kaplan et al., 2002, Molnar, et al., 2003), and for laser scanning confocal microscopy (Youngblom, et al. 2001). Though there has been significant progress in developing real-time microscopy and radiological image sharing over the internet, this has not been extended to the domain of real-time interventional manipulation of live cells, tissues, and organelles (Botvinick & Berns, 2005).

Technology is revolutionizing the biomedical field with the latest development of automatic image processing algorithms and real-time robotic devices in the study of scale of microns and even nanometers. Automated image processing algorithms have been successfully applied to tracking neurons (Cohen, et al., 1994, He, et al., 2003), Caenorhabditis elegans (Bao, et al., 2006), and sperm cells (Shi, et al., 2006a & 2006b, Nascimento, et al., 2006), identifying Sphacelaria algae (Yeom & Javida, 2006) and soil bacteria (Bloem, et al., 1995), and live embryos (Brodland & Veldhuis, 1998). Robotic telemicroscopy has been developed for general applications (Lin, et al., 2003, Botvinick & Berns, 2005) and is currently being applied to pathology (Szymas, et al., 2001, Della Mea, et al., 2000, Burgess et al., 2002) and microsurgery (Knight, et al., 2005, Kuang, et al., 2005).

Lasers are useful tools for micromanipulation of biological specimens (Prasad, 2003). With the addition of tightly focused laser beams, microscopes have been turned into elaborate tools that not only allow detailed observation of a specimen but also the capture, displacement, and microdissection of biological samples in vitro with astonishing ease and

---

[1] All three authors contributed equally to this work

accuracy (Conia, et al., 1997). Some commercial optical trapping and scissors systems are available, such as The LaserTweezers® Workstation and The LaserScissors® Workstation from Cell Robotics Inc, and PALM MicroLaser Systems from P.A.L.M. Microlaser Technologies. A review of this field is published in Methods in Cell Biology (Berns & Greulich, 2007)

We have developed a system with remote operational capabilities using several different standard microscope platforms that have evolved from a multi-parametric laser microscope described over two decades ago (Berns, et al., 1981). At that time, however, there was neither the computing power nor the internet of today, two of the key technologies that are combined with current opto-electronic microscopic systems. One goal of the "systems-integrated" microscope (RoboLase) is to develop a platform that can be accessed by collaborators via the internet. The system has been used to image, ablate, and/or trap cells and their organelles by remote-control. In the laser ablation mode (laser scissors), all the electronic components, such as the microscope, cameras, laser power and ablation coordinates, are controlled by the local host computer but can be operated by remote collaborators. Delicate microsurgery on cell organelles, such as individual microtubules, spindle fibers, chromosomes and centrioles can be performed to study each organelle's role in cell function. In addition, localized DNA damage inside the cell nucleus can be patterned to study DNA repair mechanisms. In the laser trapping (laser tweezers) mode, phase contrast images of swimming sperm are digitized to the computer at a video rate (30 frame per second) or higher (up to 90 frames per second). The custom trapping algorithm places a region of interest (ROI) centered about a sperm in response to a mouse click by a remote collaborator. All subsequent real-time tracking and trapping of the sperm are performed automatically to study relationships between sperm swimming force and swimming speed. With this system we have studied the effects of laser trap duration and power on sperm motility and are integrating real-time measurements of sperm energetics assessed by fluorescent molecules (Nascimento, et al., 2006).

2. Robotic Laser Scissors Microscope System

2.1 Microscope

The robotic laser microscope is comprised of a motorized inverted microscope stand, external optics to direct the ablation laser into the microscope, a CCD digital camera, and a hardware-software suite for the control of laser power and firing position, mechanical shutters in the laser path, the specimen stage, and microscope stand focus and illumination.

The major brands of research microscopes have all developed motorized versions of their inverted microscopes. Our system utilizes a Zeiss Axiovert 200M (Zeiss, Thornwood, NY) with motorized objective turret, reflector turret (for fluorescent filter cubes), condenser turret, halogen lamp shuttering with intensity control, mercury arc lamp shuttering, camera port selection, objective focus, and parfocality switching between objective lenses. The microscope also has a motorized optovar turret to increase the system magnification by 1.6X or 2.5X. For laser ablation experiments, a 63X, phase III, NA1.4 oil immersion microscope objective is used. The microscope stand has a built in computer which uses a controller area network (CAN) to communicate with motors and encoders within the microscope stand. The CAN can receive commands through a serial interface typically attached to a computer running an image acquisition/microscope control program. Rather than using the software provided with the microscope manufacture which we found to be cumbersome and slow,

we have developed custom control software capable of communicating with the CAN as described below.

Features of the motorized microscope that are especially relevant to remote operation of a laser microscope are the shift-free reflector turret, microscope light path selection, illumination control and objective focus. The shift-free reflector turret allows the user to repeatedly switch between any of 5 fluorescent filter cubes in the turret without a detectable pixel shift in the image. This is of great importance when performing resolution-limited targeting for laser ablation as it ensures that the laser will always focus at the expected pixel location. Likewise, the Axiovert microscope can switch from camera port to laser ablation port and back to camera port with no detectable pixel shifts when initiating an ablation sequence.

Specimens are mounted in an X-Y stepper stage (Ludl Electronic Products Hawthorne, NY) controlled with a PXI-7344 stepper motor controller (National Instruments, Austin, TX) and an MID-7604 power drive (National Instruments). The motion board is mounted in a PXI chassis (National Instruments), which is connected to the host computer through two MXI4 boards (one in the PXI chassis, the other in the host computer) through the MXI-3 fiber-optic cable (National Instruments). Motorized objective focus control is achieved through the CAN by Zeiss' Harmonic Drive DC motor providing 25nm steps with 10 mm travel for precise focus control over multiple objectives' working distances. To achieve stable temperature control for specimens imaged by an oil-immersion objective lens both the specimen and the objective lens are heated. Specimens in 35 mm Petri dishes are heated with a stage heater (heater: DH-35; controller: TC-324B; Warner Instruments Corporation, Hamden, CT) while the objective is heated with a collar-type objective heater (OBJSTD with controller, Bioptechs, inc., Butler, PA).

2.2 External laser optics and hardware

Optics outside the microscope stand guide the ablation laser into the microscope and supplies RoboLase system with automated laser power control, laser shuttering, and laser positioning (Figure 1). The laser ablation light source is a diode-pumped Vanguard with a second harmonic generator (SHG) providing TEM_{00} mode 532 nm laser light linearly polarized with 100:1 purity, 76 MHz repetition rate, 12 ps pulse duration and 2W average power(Spectra-Physics, Mountain View, CA). The unattenuated laser power is far in excess of the threshold for resolution-limited subcellular laser ablation (Botvinick, et al., 2004) and left unattenuated is well above the plasma threshold causing catastrophic damage to cells in the vicinity of the laser. We built a beam attenuator from dual linear polarizers. The laser beam polarization purity is considerably increased from 100:1 through the first glan linear polarizer (CLPA-12.0-425-675, CVI Laser, LLC, Albuquerque, NM) with a 5×10^5 extinction ratio rotated for maximum transmission (95%). Laser power is controlled by rotating an identical glan linear polarizer placed in series to the first and mounted in a motorized rotational mount driven by an open loop 2-phase stepper motor with 0.05° accuracy (PR50PP, Newport Corp, New Port, CA). The stepper motor rotates the polarizer from its vertical orientation with maximum transmission (95%) to its horizontal orientation with minimum transmission well below the damage threshold of biological samples. The stepper motor is controlled via the motion board in the PXI chassis. Light exiting the second polarizer is partially reflected by a laser-line beam sampler with dual antireflection-coated surfaces. The sampled beam is measured by a photodiode (2032 photo receiver, NewFocus,

San Jose, CA) and converted to a voltage. A calibrated photometer (1825-C, Newport Corp) is used to determine the relationship between the photodiode voltage and average laser power in the main beam. A mechanical shutter (Vincent Associates, Rochester, NY) with a 3ms duty cycle gates the main laser beam to provide 'short' bursts of pulses to the microscope (Botvinick & Berns, 2005).
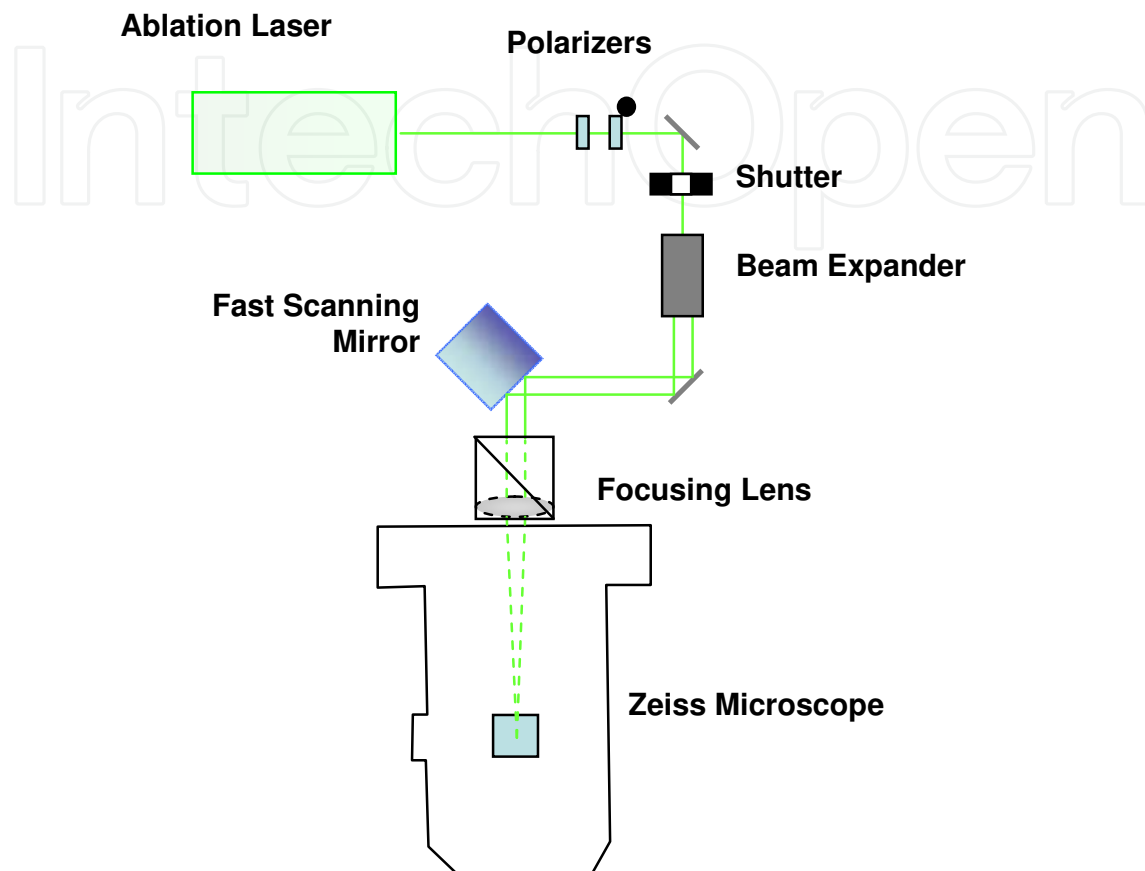

Figure 1. External laser light path of robotic laser scissors microscope system

The laser beam is then expanded using an adjustable-beam expander (2-8X, 633/780/803nm correction, Rodenstock, Germany) and lowered to a height just above the optical table by two additional mirrors. Telecentric beam steering is achieved by placing a dual-axis fast scanning mirror (Newport Corp) at an image plane conjugate to the back focal plane of the microscope objective. This image plane is formed by a 250 mm biconvex lens positioned with its front focal plane at the image plane of the microscope Keller-Berns camera port (We refer to the entry port underside the microscope as the Keller-Berns port as opposed to the Keller-port because the first Zeiss microscope with this port was built by Zeiss following the design requirements of Berns for the construction of the LAMP CATS microscope in the early 1990's (see Berns, et al., 1998). In order to access the Keller-Berns port, the microscope is raised 70 mm above the table via custom machined metal alloy posts to leave room for a 45° mirror which vertically redirects incident laser light running parallel to the table through the Keller-Berns port. Once inside the microscope stand, the laser light passes through the tube lens and one of the five fluorescent filter cubes of the reflector turret before entering the back of the objective lens. The reflector turret can be set up either with one filter slot blank, or since the turret is automated, the system can position a fluorescent filter cube into place

with appropriate laser transmission characteristics. All external mirrors in the ablation laser light path are virtually loss-less dielectric mirrors optimized for 45° reflections of 532nm S-polarized light (Y2-1025-45-S, CVI Laser LLC). It is important to note that the selection of the laser for RoboLase system was based upon our desire to produce cellular damage using multiphoton processes of the picosecond green second harmonic wavelength. We have built several other RoboLase systems using other short-pulsed lasers, such as the femtosecond Titanium sapphire laser at 800 nm (see Botvinick, et al., 2005, Wakida et al, 2006 and Gomez-Godinez, 2007).

2.3 Cameras

A high quantum efficiency digital camera is used to capture transmitted and fluorescent images. RoboLase implements a Hamamatsu Orca-AG deep-cooled 1344 x 1024 pixel, 12-bit digital CCD camera with digital (fire wire) output (Hamamatsu Photonics, K.K., Hamamatsu, Japan). The ORCA can read out sub regions of the chip for increased frame rates, bin pixels for increased signal-to-noise, and adjust gain and exposure time to trade off between signal-to-noise characteristics and arc lamp exposure times. RoboLase uses Hamamatsu's Video Capture Library for LabVIEW (ver 1.0) communicate with the ORCA camera controller through its DCAMAPI driver.

2.4 Software

The control software is programmed in the LabVIEW 8.2 (National Instruments) language and is responsible for control of the microscope, cameras and external light paths. The control software also manages image and measurement file storage. It communicates with the user through the graphic user interface or the 'front panel' in LabVIEW. The front panel receives user input and displays images and measurements. The control software interprets commands sent by the user into appropriate hardware calls and returns the results of that action to the front panel and/or computer's hard drive. Emphasis was placed on the design of the front panel, such that it would be easy to learn while providing the features needed to search for a cell of interest and then to perform cellular manipulation on that cell.

Figure 2 shows an image of the front panel of Robolase. The upper-left panel/tab contains laser parameter controls. This panel contains: 1) the Turn-on-Laser button to control the emission of the ablation laser inside the laser cavity, 2) the LaserShut button to control the laser's internal shutter, 3) the % Power slider to select a percent of maximum laser ablation power (100% percent corresponding to 3.5 mW at the focal spot after the objective), 4) the Scissors-Filter-Cube selector to choose the filter cube turret position during ablation, 5) two fire buttons, Cut ROI and Fire at (0,0), to fire the laser either at user-drawn positions or the center of the field respectively.

Once either fire button is pressed, the control software calls the microscope CAN to select the Keller-Berns port and the appropriate filter cube. The control software then continuously queries the CAN to ensure the completion of both actions before opening the mechanical shutter in the laser path for a pre-defined laser burst time. Beam steering is sufficiently faster than the camera port and filter turrets such that a quarry of its position prior to opening the shutter in unnecessary.

The center panel on the left of the front panel of Robolase in Figure 2 contains 5 tabs: 1) The 'Stage Ctl' tab contains left/right and up/down rockers to move the microscope stage with position feedback. A similar pair of rockers moves the microscope objective for focus

control. The 'Click and Move' control is a novel control designed to minimize exposure of the cells to the arc lamp light during stage movements. The user simply chooses the crosshairs tool from the toolbar to the left of the image and clicks on an object of interest in the image. The program then calculates that pixel's displacement from the field center and moves the stage to center the object. 2) The 'Coor List' tab allows the user to store the current position in a list or to return to any stored coordinate. It also allows the user to load an old list of coordinates, to clear the current list, or to save the current list to the hard drive. 3) The 'Cut ROI' tab contains controls for beam steering and for laser ablation through a series of z-coordinates. The user can select a shape tool (dot, line, rectangle, irregular shapes) from the tool bar and draw one or more shapes on the image. The region of interest (ROI) of that shape can be caved by firing single macropulse (one opening of the mechanical shutter which will pass multiple individual laser pulses). Since the laser causes near diffraction limited ablation (Botvinick, et al., 2004), the program calculates the number of macropulses necessary to fill in the shape based on the pixel dimensions of the shape and the pixel extent of a single diffraction-limited ablation. 4) The 'Camera Ctl' tab contains controls for camera gain, digitization offset, exposure time and binning. It also contains an area-of-interest control to only transfer image data from an area of interest defined with the rectangle tool in the image display. 5) The 'Microscope Ctl' tab contains controls for the microscope stand to select the objective, filter cube, condenser filter, optovar, and image port.

The lower panel on the left of Robolase front panel in Figure 2 contains image acquisition controls. The 'Image Acquisition' tab contains controls for exposing single images (Expose), continuous acquisition (Focus), image save and image printing. The user can select the filter cube for fluorescence image acquisition, whether to open the arc lamp during the exposure. The 'Root Directory' control specifies the top directory for file saving using our automated file naming system, and an indicator displaying the full path and name of the last saved image. The file path and name are designed to prevent accidental overwriting of data during successive operations of the program coding the file name with the current time. The 'Time Series' tab contains controls for acquiring a time series of images. The time series uses setting from the 'Image Acquisition' tab and contains controls for the number of images and the duration between images as well as an indicator of the last image saved in the time series.

The lower panel on the right of Robolase front panel in Figure 2 displays the last acquired image plus the slider to control/indicate the brightness of the halogen lamp. The upper panel on the right contains a message box and the image histogram. The message box displays important messages, such as error notifications or equipment status, and draws user attention by pulsing the large green digital LED to the left of the message box when a new message arrives. The gray box controls the image display lookup table for mapping 12-bit images to the 8-bit display. This control uses four modes of look-up table: 1) Full-dynamic, in which the range of non-zero intensities are divided into 256 equally spaced bins, 2) 90%-dynamic, in which the dynamic range containing the middle 90% of the cumulated histogram of the image is divided into 256 equally spaced bins, 3) Given-range, in which the range of grayscale values specified by the 'Maximum Value' and 'Minimum Value' slider controls are equally divided into 256 bins, and 4) Down-shift, in which the grayscale values are shifted to the right in 8-bit increments as specified by a control. An image histogram displays the pixel intensity histogram of the last acquired image to aid in the selection of an appropriate lookup table.
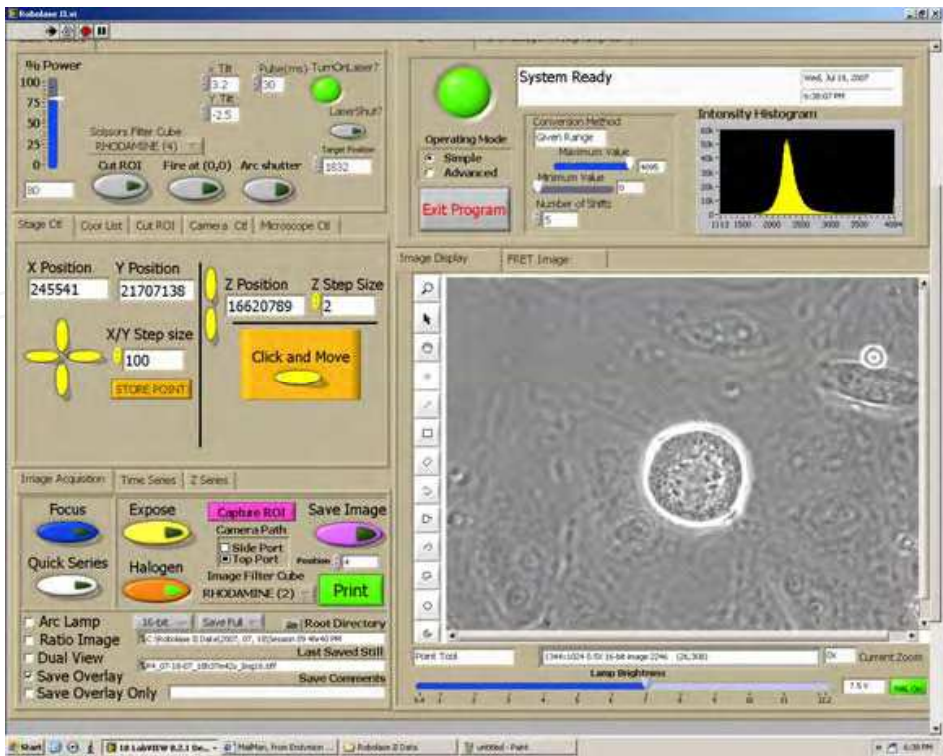
Figure 2. Front panel of robotic laser ablation microscope system

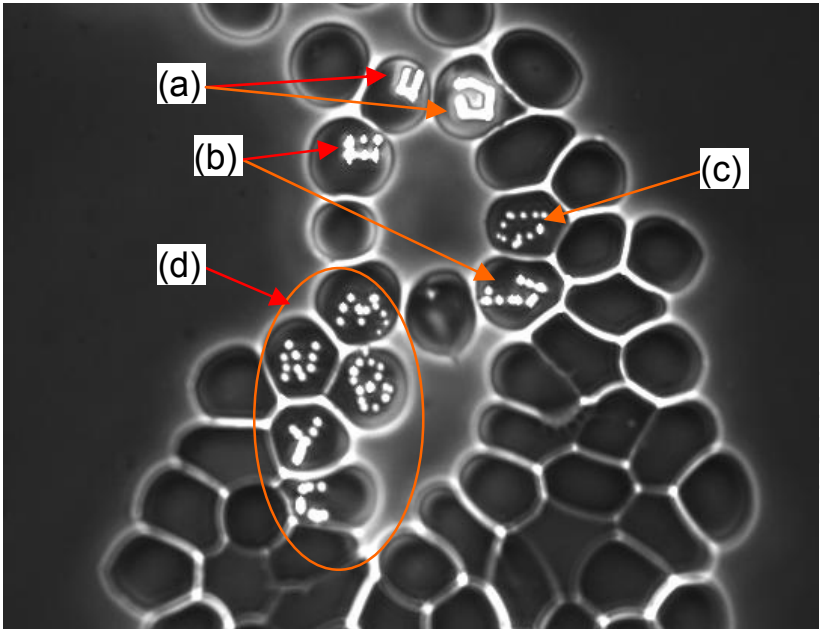## 2.5 Internet-based laser ablation control

Figure 3. Irregular shape laser cuts on red blood cells on robotic laser scissors microscope system via internet. The irregular shapes were cut out with the ablation distance smaller than the actual ablation radius (3µm) at high laser power as shown in (a). The discrete ablation spots can be clearly seen with bigger ablation distance at high laser power in (b) and at low laser power in (c). The patterns (MB and NYC) is laser-etched in 4(d) (Shi, et al., 2006c, © 2006 IEEE)

The robotic laser ablation microscope system at University of California, San Diego/Irvine can be operated via the internet using most internet accessible devices, including laptops and desktop computers. The experiment testing irregular shape cutting through the internet was conducted from New York City using the www.logmein.com web server as shown in Figure 3. Red blood cells were deposited on a microscope cover glass, allowed to air-dry, and mounted in a cell culture chambers (rose chamber, Shi, 2006a). The collaborator in New York City logged in to RoboLase system and drew multiple shapes on the captured image at San Diego. That collaborator also modified the ablation power and the ablation distance between the two ablation spots in the front panel of RoboLase as shown in Figure 3 (higher laser power and bigger ablation distance was used in (a), higher laser power and smaller ablation distance in (b), lower laser power and bigger ablation distance in (c), patterns of alphabet letters of MB and NYC were laser-etched in (d)).

3. Robotic Laser Tweezers Microscope System

The robotic laser tweezers microscope system can be designed in the robotic laser scissors microscope system similar to that discusses in Botvinick & Berns 2005 (the trapping laser was directed behind the microscope in the arc lamp illumination light path to merge the two light paths). The robotic laser tweezers microscope system may be designed and built as a stand-alone system as described in Shi, 2006c. Real-time automatic tracking and trapping of sperm (RATTS) is discussed in this paper as an example of RoboLase system.

3.1 Hardware and optical design of RATTS

A single point gradient trap was generated using a Nd:YVO$_4$ continuous wave 1064nm wavelength laser (Model BL-106C, Spectra Physics) coupled into a Zeiss Axiovert S100 microscope and a 40x, phase III, NA 1.3 oil immersion objective. The optical design is shown in Figure 4. Laser light is reflected off two dielectric mirrors to orient the beam parallel to the table and along the optical axis of the microscope. The beam is expanded by two lenses (plano-concave lens, f = -25.5mm at λ = 1064nm, and plano-convex lens, f = 76.2mm at λ = 1064 nm) in order to fill the objective's back aperture. A third lens (biconvex lens, f = 200mm) focuses the beam onto the side port of the dual video adaptor to ensure the beam is collimated at the objective's back aperture. The dual video adaptor contains a filter cube with a dichroic mirror that allows laser light entering the side port to be transmitted to the microscope while reflecting visible light to the camera attached to the top port for imaging. A low pass filter (D535/40M, Chroma Technology Corp., Rockingham, VT) is placed in the filter cube to block back reflections of IR laser light while allowing visible light to pass. The laser trap remains stationary near the center of the field of view. In order to trap a sperm the microscope stage is moved to bring the sperm to the laser trap location. The laser trap location is determined prior to each experiment by trapping 10µm-diameter polystyrene beads suspended in water within a 35 mm diameter glass bottom Petri dish. The trap depth within the sample is kept to approximately 5 µm (approximately one sperm head diameter) above the cover glass. This ensures that the trap geometry is not sensitive to spherical aberrations from the surrounding media (Nascimento, et al., 2006). Laser power in the specimen plane is attenuated by rotating a polarizer (**CVI Laser LLC**) that is mounted in a stepper-motor-driven rotating mount (PR50PP, Newport Corp). The mount is controlled by a custom program that allows the experimenter to set the power decay rate (rotation rate of

polarizer) and record laser power at the moment a sperm escapes the trap. The specimen is imaged by a CCD camera (XC – 75, Sony, Sony, Japan operating at 30 frames per second or Cohu, Model 7800, San Diego, CA, operating up to 90 frames per second), coupled to a variable zoom lens system (0.33 – 1.6 X magnification) to demagnify the field of view. For video rate RATTS operation, analog output (RS-170 format) from the Sony CCD is distributed to a TV monitor, a Camcorder (DCR-PC101, Sony, Japan) for recording, and the image acquisition board PXI-1409 (National Instruments) through a video distribution amplifier (IN3218HR,Extron Electronics, Anaheim, CA). For cases to acquire the sperm swimming images in higher frame rate, the digital output (RS-422 format) from the Cohu camera is connected to the 16-bit digital image acquisition board PCI-1422 (National Instrument) for image display and streaming. Note that only one camera is used at a time in RATTS.
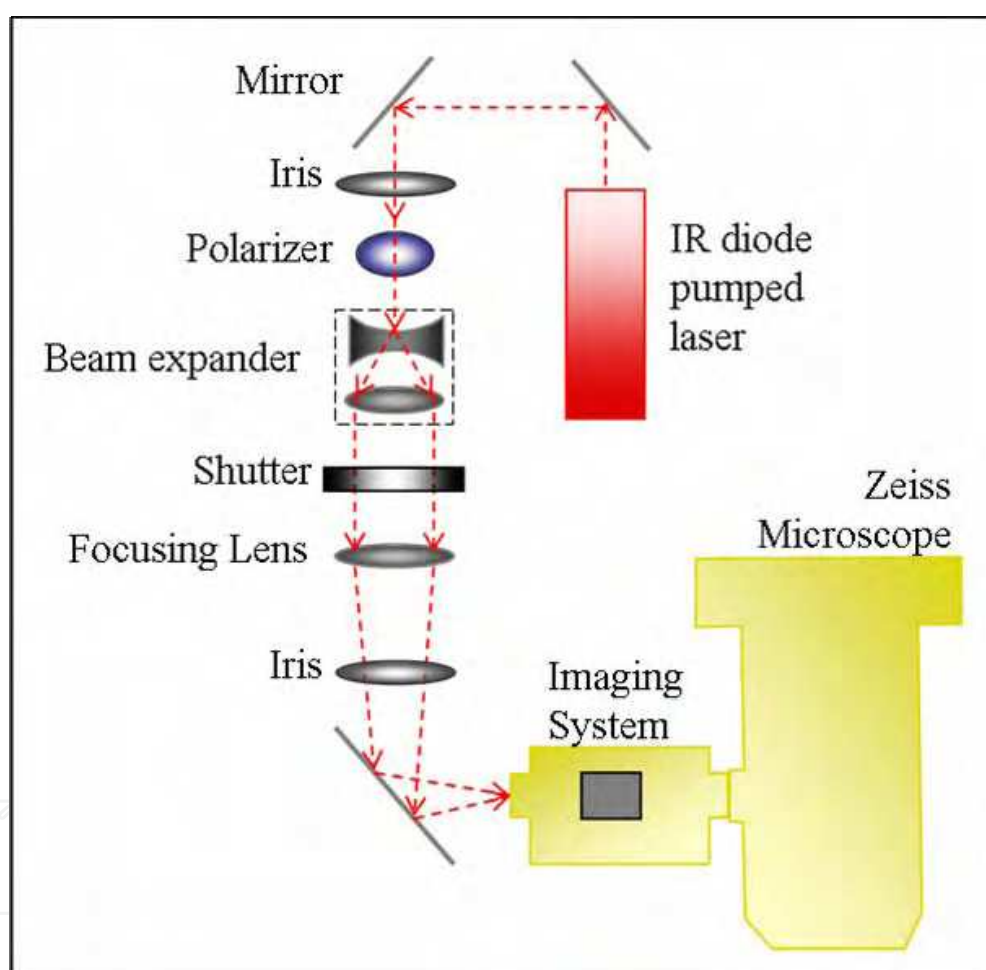
Figure 4. External laser light paths of robotic laser trapping microscope system

3.2 Software design of RATTS
RATTS is custom coded in the LabView 8.2 language (National Instruments) to process streaming images, calculate sperm trajectories, and drive the motion hardware (Shi, et al, 2006b). RATTS implements the image segmentation and sperm tracking algorithm (SSTA) in real time (Shi et al., 2006a). Images are digitized by the image acquisition board and transferred into a continuous buffer from which they are retrieved for image analysis and

displayed in the front panel as shown in Figure 5. The bright dots in the image window are living sperm in a rose chamber. The command tab allows the user to define different features in the experiment:

1. AutoStop: if checked, RATTS will track a sperm for pre-defined duration. If not checked, RATTS will track the sperm until the user press StopTracking or StropProgram button.
2. RealTime: if checked, the live images of sperm swimming are acquired and displayed on the front panel. If it is not checked, RATTS will load the saved image based on the directory in SSTA tab.
3. Decay: if checked, laser power is decayed after a sperm is trapped. Parameters are entered for maximum (or constant) laser power, rate of power decay, and if appropriate, duration of the trap in the Decay tab. If Decay is not checked, the laser power is held constant (0-420 mW at focal spot after the objective) for a fixed duration in the trapping phase of the experiment.

During real-time experiments, image analysis detects when a tracked sperm has reached a defined rectangular boundary near the extremity of the field of view. RATTS moves the microscope stage to position the sperm centroid at the center of the field of view. If Chase is checked (in command tab, Figure 5), the sperm centroid position is extrapolated using a multi-thresholding method to predict the sperm's position beyond the most recent image in order to compensate for swimming during the stage movement. Swimming parameters are calculated and saved in a continuously updated data file. Since new images arrive at 30 (or up to 90) frames per second, it is necessary to restrain net computation and data writing time to less than 33 ms (or less for the higher frame rates) in order to capture and process each image. RATTS is coded to use the most recent frame in the buffer. Sperm were recorded and tracked for extended durations to demonstrate variability in swimming parameters and variation in the swimming speed as a function of track length and track time.

The automated trapping mode of RATTS replaces our manual protocol as previously described (Nacimental, et al., 2006). User input is limited to setting parameters prior to an experiment and selecting, via the computer mouse, a sperm for analysis within the continuously updated image display. During the experiment, the user selects a sperm to be analyzed by clicking on its image with the arrow curser on the front panel of RATTS in Figure 5. The curser coordinate is registered, passed to the tracking algorithm and computation proceeds with no further intervention. Once the specified number of frames has been processed, the stage is moved to place the sperm under the laser trap and the shutter is opened.

During the trapping phase of the experiment, RATTS implements an escape detection subroutine to detect the presence of a sperm in the laser trap and to respond if the sperm escapes the trap. The subroutine monitors a small square pixel region (representing approximately 10 µm per side) centered about the laser trap. Using SSTA algorithms (Shi, et al., 2006a), the subroutine segments the image within this region and uses size threshold to detect the presence or absence of a sperm. A sperm must remain in the trap for a continuous 15 frames or the subroutine declares a failed trapping attempt.

During constant-power trapping experiments, the escape detection subroutine is used to ensure that, the sperm was successfully trapped, and second that it does not escape the trap during the trapping phase of an experiment. If the sperm is not initially trapped, RATTS will

use the SSTA algorithm to again find the sperm and continue tracking it for a user-defined number of frames after which a new trapping attempt is made. RATTS will repeat this either until the sperm is trapped, or for a user-defined number of attempts. If a sperm escapes before the trap duration is completed, the algorithm will continue to track that sperm and attempt to re-trap it.
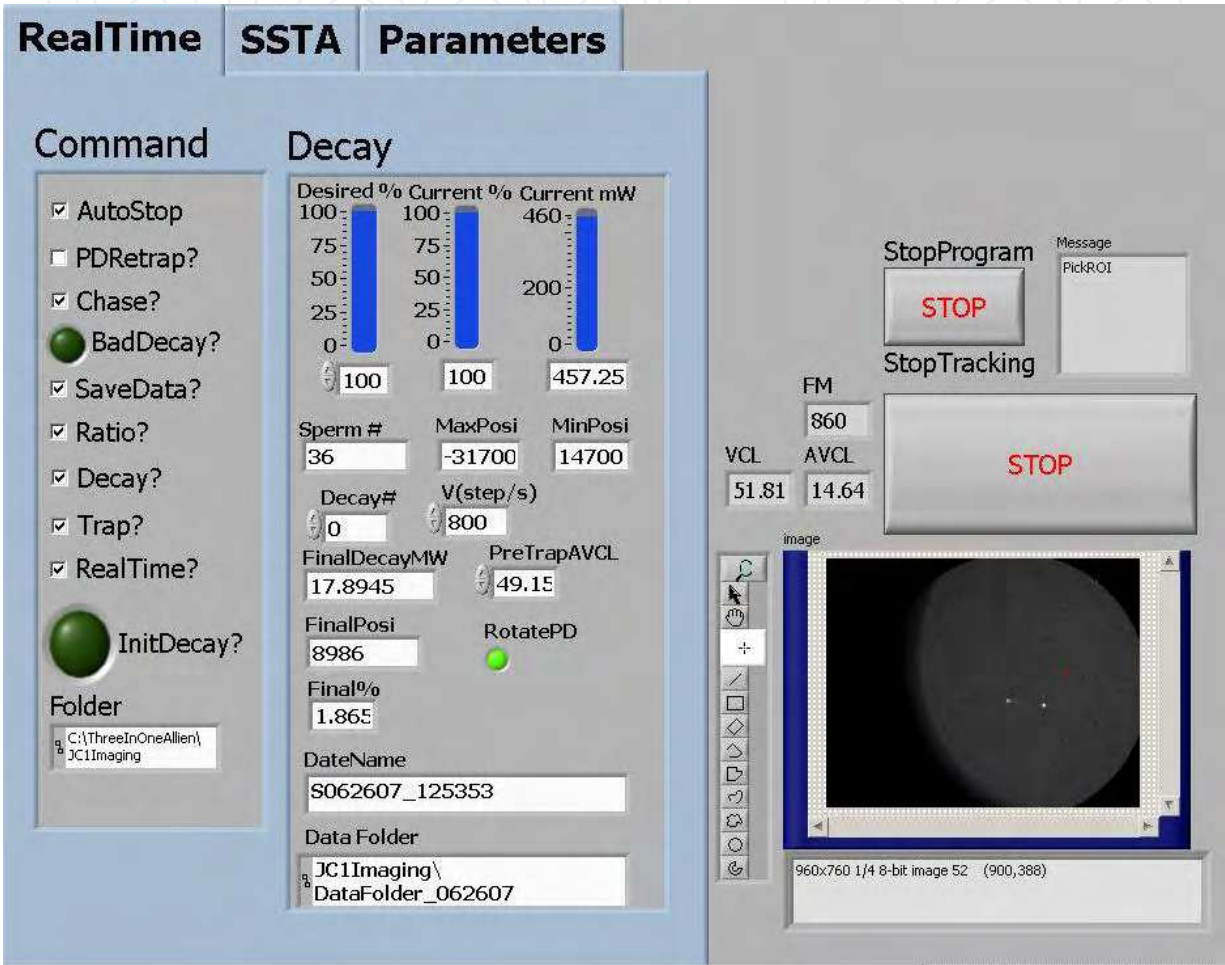

Figure 5. Front panel of RATTS system

In power decay experiments, the escape detection subroutine is used to ensure that a sperm is stably trapped. The laser power used to first trap a sperm is a user-defined percentage of maximum power (or maximum transmission through the polarizer). Once a sperm is stably trapped, RATTS automatically decays the laser power by rotating the polarizer until the sperm is capable of swimming away from the trap. Once the escape is detected, the polarizer position (and thus laser power) is written to hard disk and the polarizer is automatically rotated back to its starting position. A running file is updated at video rate or higher to record real-time swimming parameters including frame-by-frame centroid coordinates, position, and escape power. Figure 6 shows a flow diagram of the RATTS algorithm for power decay experiments.
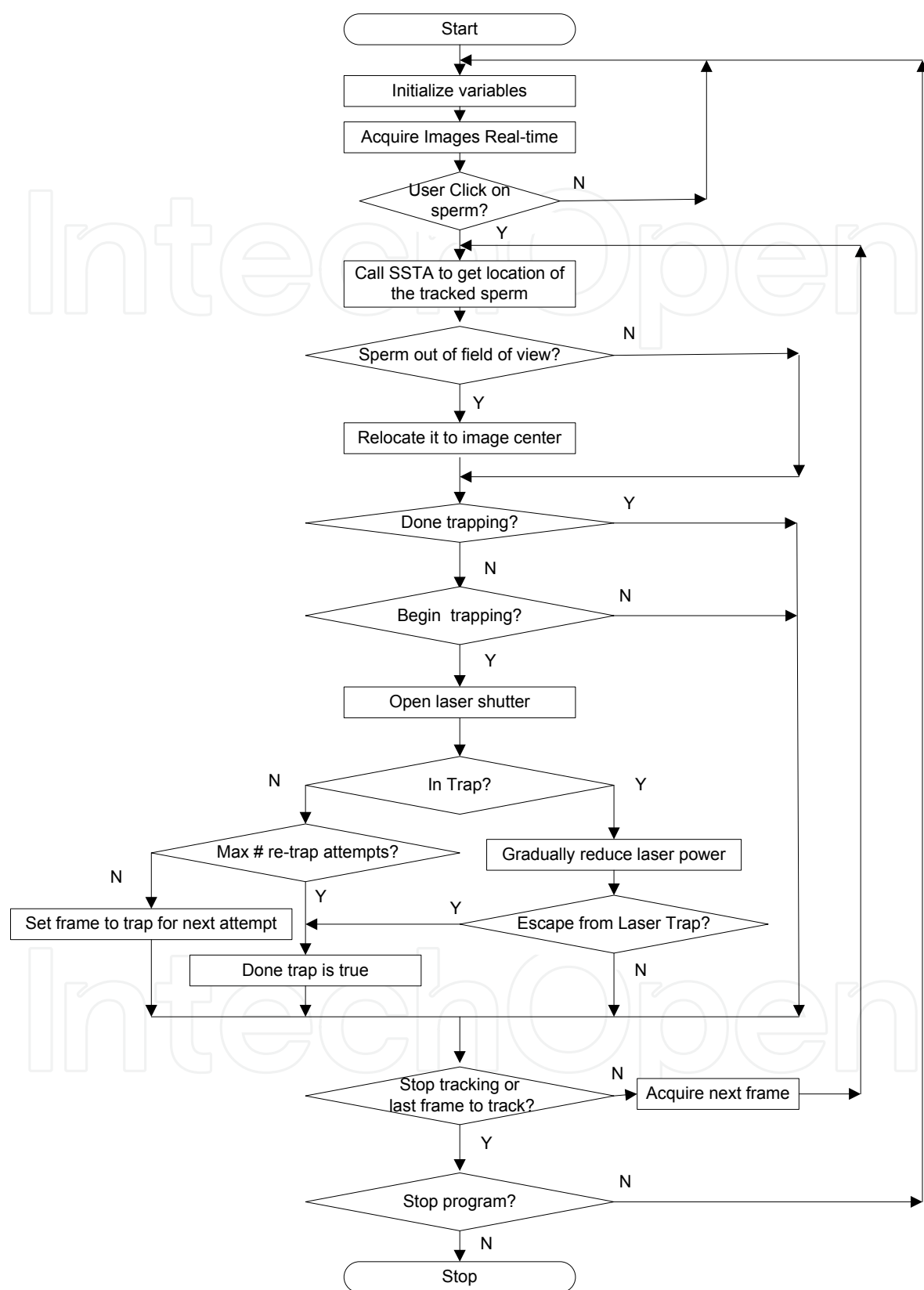
Figure 6. Flowchart of RATTS in power decay mode using the robotic laser tweezers microscope system (Shi, et al., 2006b)

4. Biological Experiments using Robolase Systems

The robotic laser scissors microscope system has been used to perform nano-surgery on both single microtubules as well as microtubule spindles in living cells (Botvinick & Berns, 2004, Wakida, et al., 2006, Conia, et al., 1997, Baker, et al., 2006, Shi, et al., 2006c). As Figure 7 demonstrates, a diffraction limited spot within a single fluorescent microtubule (transfected with a cyan fusion protein)in a live rat kangaroo kidney epithelial cell (Ptk2) can be ablated and the post-irradiation depolymerization can be observed in subsequent images . The single microtubule (Figure 7(a)) was positioned under the laser ablation crosshairs as shown in Figure 7(b). By pressing the "Fire at (0,0)" button (Figure 2), a 20ms macropulse (Botvinick, et al. 2004) was delivered to the microtubule. Figure 7(c-f) showed the microtubule depolymerizing at 1 s (Figure 7(c)), 5 s (Figure 7(d)), 10 s (Figure 7(e)), and 15 s (Figure 7(f)) post ablation.
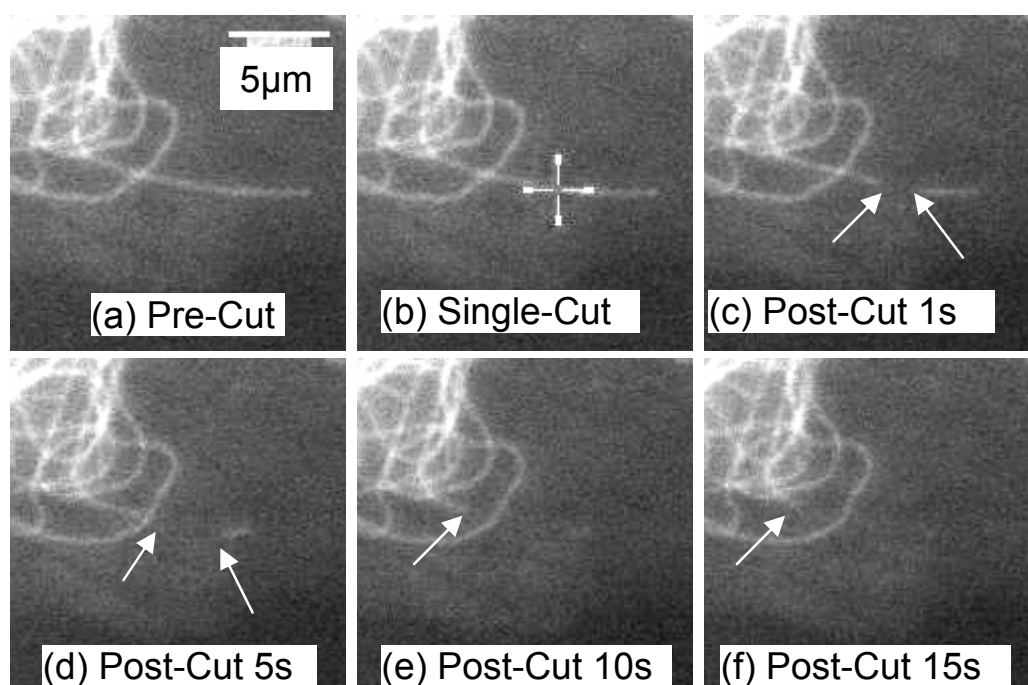
Figure 7. Effects on single microtubule of PTK2 cells using robotic laser scissors system. (a) Fluorescent image before laser exposure. (b) Crosshairs depict exact location of laser focal point during laser exposure. (c-f) Images captured immediately after laser exposure show a loss of fluorescence in the targeted region. (Shi, et al., 2006c, © 2006 IEEE, images courtesy of Nicole Wakida, University of California, Irvine)

Experiments using the robotic laser scissors microscope system have also shown that ablation across both mitotic half spindles (severing microtubule connections between the spindle pole and chromosome at the metaphase plate) immediately after anaphase-onset results in either the prevention or delay of cytokinesis. The machinery by which chromosomes move from the metaphase plate to the poles appeared to be unaffected in cells of the rat kangaroo line (PTK2) stably transfected by ECFP-tubulin (Figure 8). Anaphase onset can be observed in either phase contrast (Figure 8(a)) or fluorescence (Figure 8(b)) microscopy. The experimenter draws two rectangular regions of interest (Figure 8(c, d)) each of which are scanned by the ablation laser. Figure 8(e) shown a fluorescent image

acquired 90 seconds after ablation demonstrating recovery of the mitotic spindle. The chromosomes still underwent pole-ward anaphase movements via spindle contraction as shown in the phase contrast (Figure 8(f)) and fluorescence (Figure 8(g)), but cytokinesis did not occur after several hours as shown in Figure 8(h).
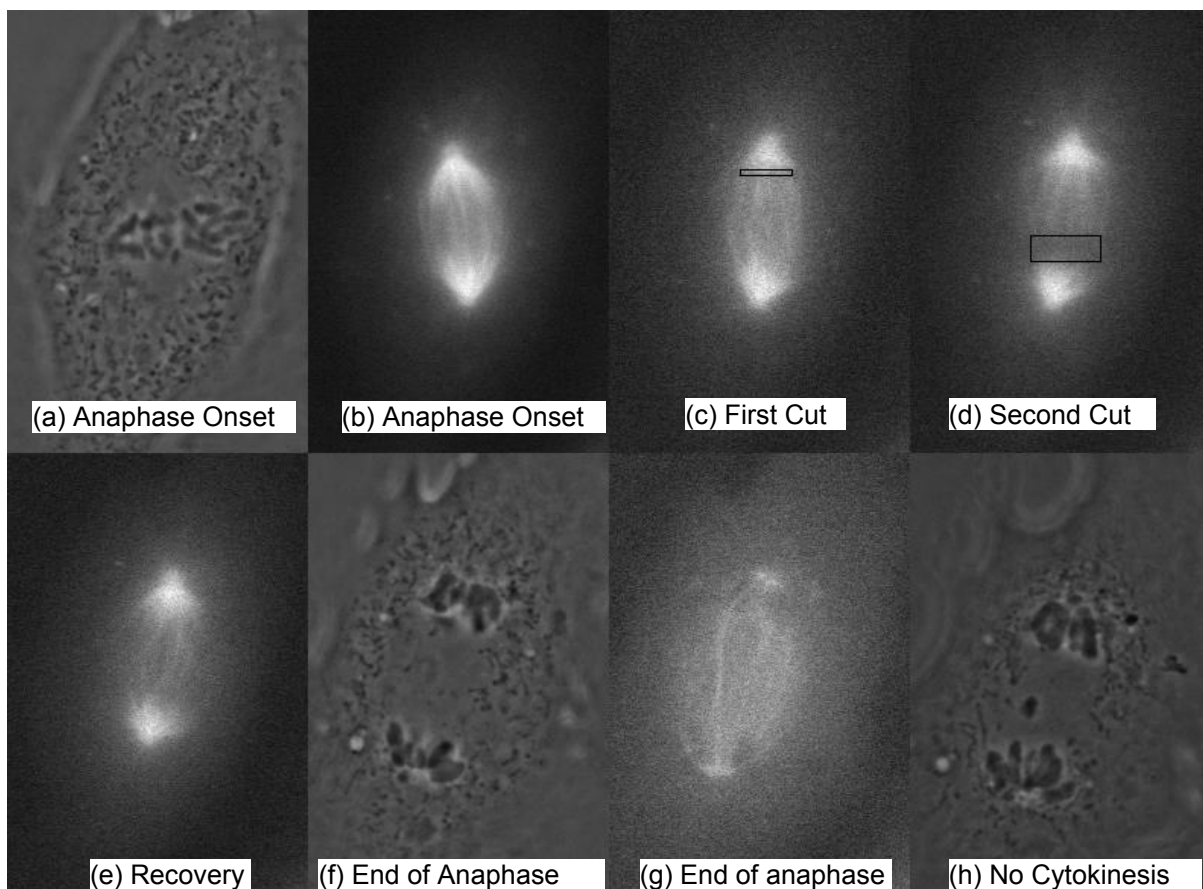

Figure 8. Anaphase spindle cutting of PTK2 cells using robotic laser scissors system. (a) Anaphase onset shown in phase contrast image. (b) Fluorescence image of anaphase onset. (c) Fluorescent image after the first cut. (d) Fluorescent image after the second cut. (e) Fluorescent image during recovery. (f) Phase contrast image at end of anaphase. (g) Fluorescent image at end of anaphase. (h) No cytokinesis after several hours (Shi, et al., 2006c, © 2006 IEEE, images courtesy of Norman Baker, University of California, San Diego)

The robotic laser tweezers microscope system has been used to study the sperm motility and swimming force (RATTS). RATTS can track and trap fast moving sperm in real-time (Figure 9). The continuous tracking mode can track single sperm over long durations. The longest duration we achieved was 11260 frames (6.25 min) for a dog sperm; its swimming trajectory is shown in Figure 9(a) (Note that the average survival time after the dog sperm is loaded to the microscope is about 20 min). The swimming trajectory of the sperm appears to be a relatively straight line when viewed in a stationary field of view as shown in the rectangle box (lower right corner) in Figure 9(a). The curvilinear velocity (VCL) in Figure 9(a) is 52 μm/s. Figure 9(b) shows an example of a single sperm tracked for 3 seconds, trapped it for 10 seconds (at 350 mW at focal spot), released, and tracked again for 3 seconds. The sperm changed swimming direction after laser trapping.

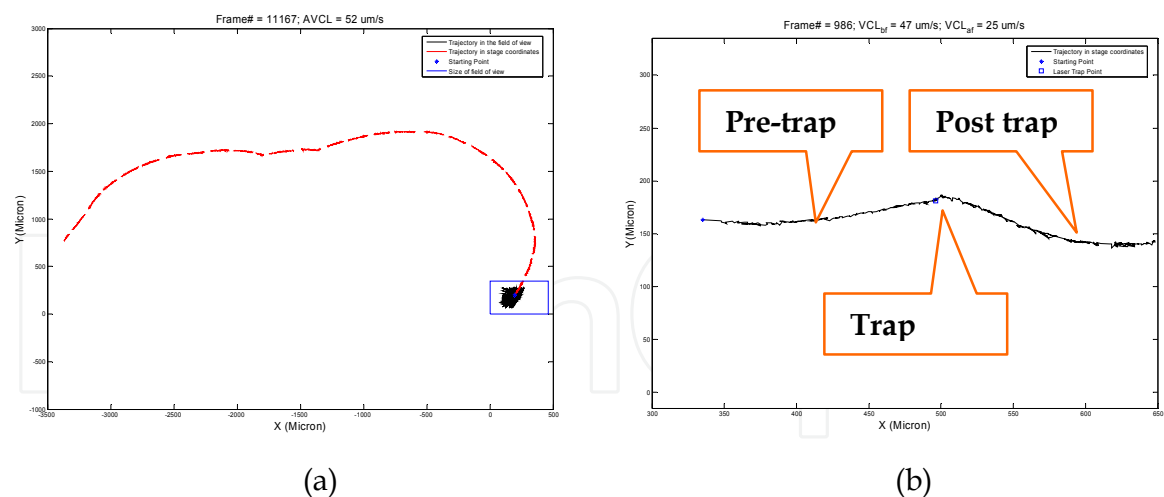(a)   (b)

Figure 9. Sperm trajectories using laser tweezers system. (a) Continuing tracking of single sperm for 6.25 min (b) Track and trap single sperm (Shi, et al., 2006b)
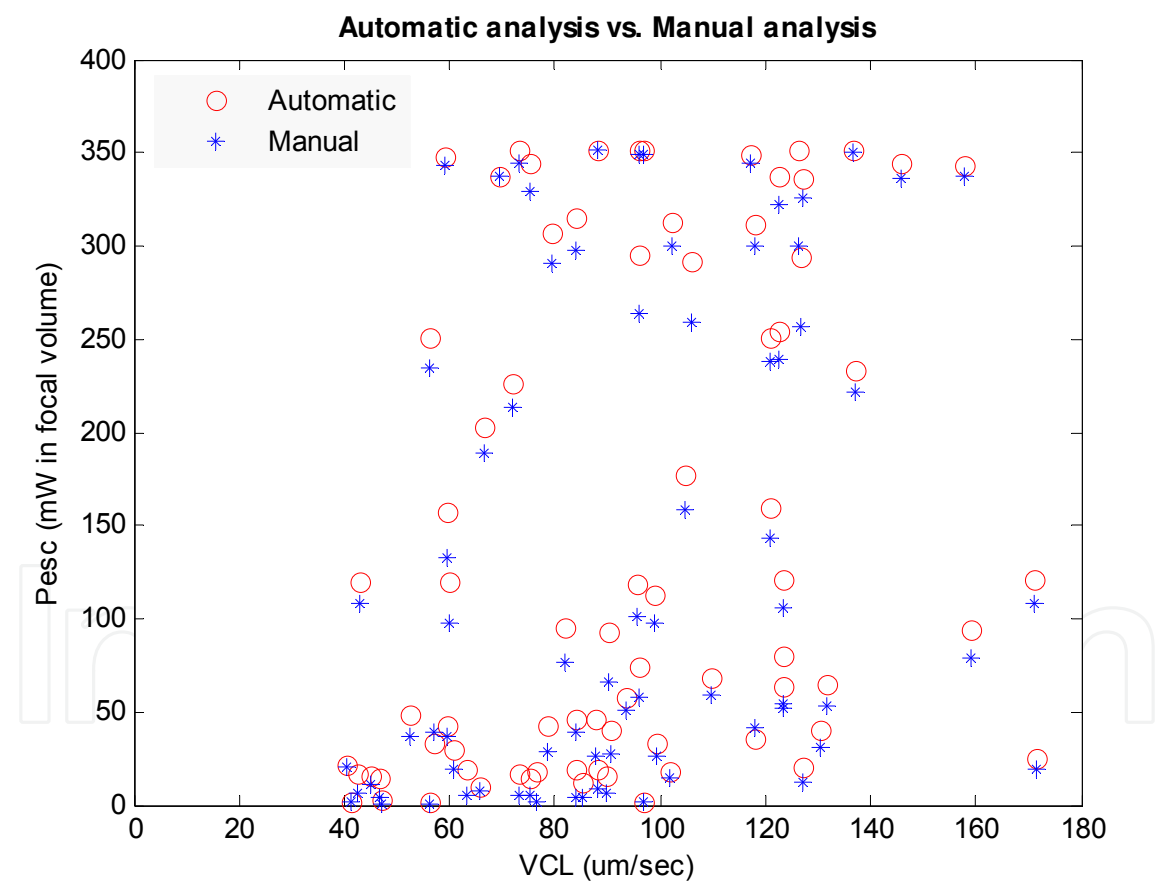

Figure 10. Escape power assessed manually and automatically. The scatter plot shows escape power determined by RATTS (∘) and by user mouse click (*) as a function of curvilinear swimming speed (VCL). Delay time is defined as the RATTS measurement minus the manual measurement. Delay times between RATTS and manual detection of escape had a mean and standard deviations of [0.46, 0.4] seconds with delays as long as 3

seconds. Scatter plots (not shown) of error against either VCL or the RATTS measurement show no non-linear relationship. Linear regression of errors as a function of VCL yields [slope = 0.06, R^2 = 0.04, p = 0.1], which casts doubt on a non-random relationship. Linear regression of errors against the RATTS measurement yields [slope = 0.02, R^2 = 0.05, p < 0.05], which indicates a very weak relationship, if any, with poor predictive power. Thus manual measurements cannot be corrected retrospectively (Shi, et al., 2006b)

To compare escape power measurements assessed manually or by RATTS, a subroutine was written to record the polarizer orientation when escape is register by the user (register as a mouse click) and by RATTS. The power decay continues until both RATTS and the user respond. Latency in the human response result in negatively biased laser power measurements since the polarizer continues to rotate until the mouse is clicked. Figure 10 shows escape laser power of each individual sperm measured manually (*) and by RATTS (○). Manual measurements were less than or equal to those of RATTS 95% of the time. Delay times between RATTS and manual detection of escape had a mean and standard deviations of [0.46, 0.4] seconds with delays as long as 3 seconds (Shi, et al, 2006b).

The RATTS system can also be accessed through the internet (Logmein.com server) as showed in Figure11. Collaborators from the University of Queensland, Brisbane, Australia accessed RATTS. Dog sperm were loaded into a rose chamber and onto the Robolase at University of California, San Diego. Images of the sperm swimming were seen in Australia through the internet. One of the collaborators in Australia clicked on a swimming sperm "of-choice" (Figure 11(a)) to initialize the RATTS to track the sperm for the next 5 seconds. The sperm was then relocated to the laser trap position and held under the trap (410 mW at focal spot) for 10 seconds (Figure 11(b)).
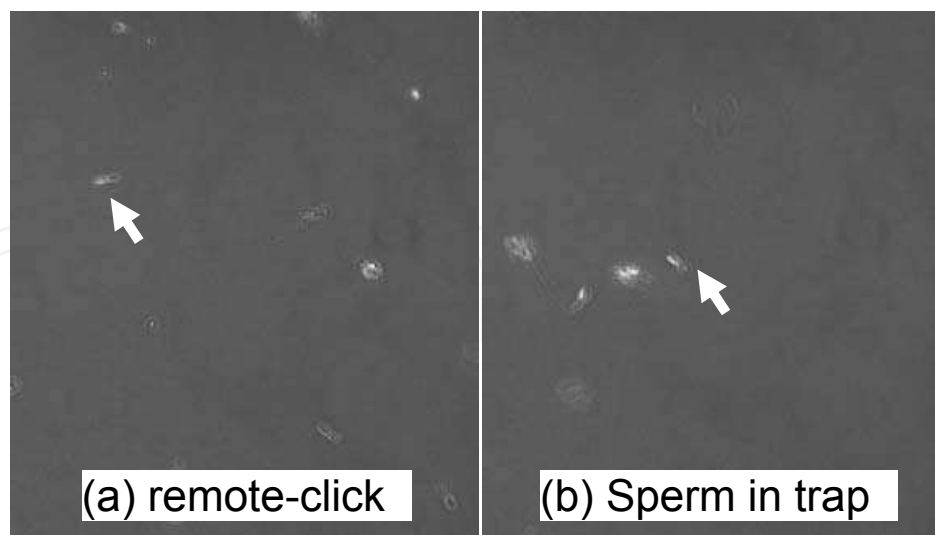

Figure 11. Remote-control of RATTS. (a) Collaborator from Australia clicked on a selected swimming dog sperm on the image screen in Australia which then activated RATTS in the UCSD lab. (b) The same sperm in (a) was held in the laser trap after tracking it for 5 seconds. It was trapped for 10 seconds (Shi, et al., 2006c, © 2006 IEEE)

5. Conclusion and future work

In this paper, the structure and features of the robotic laser scissors and laser tweezers microscope systems are presented. The Robolase systems are shown to be accessible through the internet using the Logmein program, making it feasible to perform biological experiments with remote collaborators. Future developments may involve the creation of separate log-in software for simultaneous use by more than two users/collaborators as well as the use of dedicated fiber-optic lines between different locations.

The robotic laser scissors microscope system can be used to ablate a single microtubule and to study the subsequent depolymerization. Ablating of both mitotic half spindles immediately after anaphase-onset was shown to prevent or delay cytokinesis while preserving chromosome pole-ward movement. We demonstrated that the robotic laser tweezers microscope system can be used to study sperm motility by integrating real-time measurements of swimming parameters and laser tweezers assessment of swimming force. To facilitate remote operation of experiments, the user is allowed to select from different types of sperm analysis experiments: continuous tracking experiments to measure motility within a population, track and trap experiments at constant power to determine affects on sperm motility, and track and trap experiments with decaying laser power to study the relationship between sperm motility and sperm swimming force.

The RoboLase systems are now being used in a variety of other biological experiments, including the molecular mechanism of DNA repair. Since the laser ablation can generate patterned DNA damage in defined areas of the nucleus at defined points in the cell cycle (Lisby & Rothstein, 2004), it is becoming a very powerful tool to study DNA repair mechanisms (Gomez-Godinez, et al., 2006). The studies involve studying the molecular mechanisms underlying the activation of checkpoints and the control of the progression through the cell cycle following laser-induced DNA damage (results not shown). Note that different pulse energies and irradiances will produce different damage modalities, and likely recruit different repair molecules. The Robolase project is pursuing this in multiple Robolase systems with nano, pico, and femto second lasers, as well as cw UV lasers (Chen, et al., 2005, Wakida, et al., 2006, Gomez-Godinez, et al., 2006, Baker, et al., 2006).

7 References

Baker, N. M., Botvinick, E. L., Shi, L. Z., Wu, G. & Berns, M. B. (2006). Mitotic spindle studied using laser scissors, *SPIE Optics & Photonics conference*, San Diego, August 2006, 6326.

Bao, Z., Murray, J. I., Boyle, T., Ooi, S. L., Sandel, M. J. & Waterston, R. H. (2006). Automated cell lineage tracing in Caenorhabditis elegans. *Proc Natl Acad Sci*, U S A., February 2006, Vol. 103(8), pp. 2707–2712

Berns, M. W. & Greulich, K. O (2007). *Laser Manipulation of cells and tissues. In Methods in Cell Biology*. Academic Press Inc. ISBN-13: 978-0-12-370648-5, San Diego, CA, USA.

Berns, M. W., Tadir, Y., Liang, H. & Tromberg, B. (1998) *Laser scissors and tweezers. In: Methods in Cell Biology*. M. P. Sheetz (ed.). Academic Press, Inc, San Diego, CA, Vol. 55, pp. 71-97.

Berns, M. W., Botvinick, E. L., Liaw, L., Sun, C-H. & Shah, J. (2005). Micromanipulation of chromosomes and the mitotic spindle using laser microsurgery (laser scissors) and laser-induced optical forces (laser tweezers), *Cell biology: a laboratory handbook*. Burlington, MA: Elsevier Press

Bloem, J., Veninga, M. & Shepherd, J. (1995). Fully Automatic Determination of Soil Bacterium Numbers, Cell Volumes, and Frequencies of Dividing Cells by Confocal Laser Scanning Microscopy and Image Analysis. *Appl Environ Microbiol.* Vol. 61(3), pp. 926-936

Brodland, G. W. & Veldhuis, J. H. (1998). Three-dimensional reconstruction of live embryos using robotic macroscope images. *IEEE Trans Biomed Eng.* Vol. 45(9), pp. 1173-1181

Botvinick, E. L. & Berns, M. W. (2005). Internet-based robotic laser scissors and tweezers microscopy, *Microsc Res Tech.* Vol. 68(2), pp. 65-74

Botvinick, E.L., Venugopalan, V., Shah, J.V., Liaw, L.H., Berns, M,W.(2004). Controlled ablation of microtubules using a picosecond laser.*Biophys J.* Vol. 87(6), pp. 4203-12

Burgess, J. R., Sandberg, G. D., Myers, C. P., Bigott, T. R. & Greenspan, R. B. (2002). Use of robotic telepathology for frozen-section diagnosis: a retrospective trial of a telepathology system for intraoperative consultation, *Mod Pathol.* Vol. 15(11), pp. 1197-1204

Chen, B. P.C., Chan, D. W., Kobayashi, J., Burma, S., Asaithamby, A., Yano, K., Botvinick, E. F., Qin, J. & Chen, D. J. (2005). Cell cycle dependence of DNA-PK phosphorylation in response to DNA double strand breaks. *J. Biological Chemistry*, Vol: 280, pp. 14709-15

Chumbley L.S., Cassucio G., Kritikos D., Lentz H., Mannes C. & Mehta K. (2002). Development of a web-based SEM specifically for K-12 education. *Microsc Res Tech*, Vol. 56(6), pp.454-461

Cohen, A. R., Roysam, B. & Turner, J. N. (1994). Automated tracing and volume measurements of neurons from 3-D confocal fluorescence microscopy data. *J Microsc.* Vol. 173(2), pp. 103-14

Conia, J., Edwards, B. S. & Voelkel, S. (1997). The micro-robotic laboratory: optical trapping and scissing for the biologist, *J. Clin Lab Anal.*, Vol. 11(1), pp. 28-38

Della Mea, V., Cataldi, P., Pertoldi, B. & Beltrami, C. A. (2000). Combining dynamic and static robotic telepathology: a report on 184 consecutive cases of frozen sections, histology and cytology, *Anal Cell Pathol*. Vol. 20(1), pp. 33-39

Gomez-Godinez, V., Wakida, N. M., Dvornikov, A. S., Yokomori, K. & Berns, M.W. (2007). Recruitment of DNA damage recognition and repair pathway proteins following near-IR femtosecond laser irradiation of cells. *J Biomed Opt*. Vol. 12(2), 020505

Hadida-Hassan M., Young S. J., Peltier S. T., Wong M., Lamont S. & Ellisman M. H. (1999). Web-based telemicroscopy. *J Struct Biol*. Vol. 125(2-3), pp. 235-245

He, W., Hamilton, T. A., Cohen, A. R., Holmes, T. J., Pace, C., Szarowski, D. H., Turner, J. N. & Roysam, B. (2003). Automated Three-Dimensional Tracing of Neurons in Confocal and Brightfield Images. *Microsc Microanal*. Vol. 9(4), pp. 296-310

Kaplan K. J., Burgess J. R., Sandberg G. D., Myers C. P., Bigott T. R. & Greenspan R. B. (2002). Use of robotic telepathology for frozen-section diagnosis: a retrospective trial of a telepathology system for intraoperative consultation. *Mod Pathol*. Vol. 15(11), pp. 1197-1204.

Knight, C. G., Lorincz, A., Cao, A., Gidell, K., Klein, M. D. & Langenburg, S. E. (2005). Computer-assisted, robot-enhanced open microsurgery in an animal model, *J Laparoendosc Adv Surg Tech A*. Vol. 15(2), pp. 182-185

Kuang, W., Shin, P. R., Oder, M. & Thomas Jr. A. J. (2005) Robotic-assisted vasovasostomy: a two-layer technique in an animal model. *Urology*. Vol. 65(4), pp.811-814

Lin, W., Wilder, J., Grossman, S. & Foran, D. J. (2003). A network-reactive model for distributed telemicroscopy. *J Telemed Telecare*. Vol. 9(2), pp. 78-83

Lisby, M. & Rothstein R. (2004). DNA damage checkpoint and repair centers, Current opinion in Cell Bio., Vol. 16, pp. 328-334.

Parkin S., Knöner G., Singer W., Nieminen T. A., Heckenberg N. R., Rubinsztein-Dunlop H. (2007). Optical torque on microscopic objects. *Methods Cell Biol*. Vol. 82, pp. 525-61

Prasad, P. N., (2003). *Introduction to biophotonics*, John Wiley & Sons, Inc., Hoboken, New Jersey

Molnar B., Berczi L., Diczhazy C., Tagscherer A., Varga S. V., Szende B. & Tulassay Z. (2003). Digital slide and virtual microscopy based routine and telepathology evaluation of routine gastrointestinal biopsy specimens. *J Clin Pathol*, Vol. 56(6), pp.433-438

Nascimento, J. M., Botvinick, E. L., Shi, L. Z., Durrant, B. & Berns, M. W. (2006). Analysis of sperm motility using optical tweezers. *J. Biomed Opt.*, Vol. 11(4), 044001

Shi, L. Z., Nascimento, J. M., Berns, M. W. & Botvinick, E. L. (2006). Computer-based tracking of single sperm. *J. Biomed Opt,* Vol. 11(5), 054009

Shi, L. Z., Nascimento, J. M., Chandsawangbhuwana, C., Berns, M. W. & Botvinick, E. L. (2006). Real-time Automated Tracking and Trapping System (RATTS) for Sperm. *Microsc Res Tech*. Vol. 69(11), pp. 894-902

Shi, L. Z., Nascimento, Wakida, N., Dvornikov, A., Baker, N., Botvinick, E. L. & Berns, M. W. (2006). "RoboLase", A robotic laser scissors and laser tweezers microscope. *40th Asilomar Conference on Signals, Systems, and Computers*, pp. 173-177, Asilomar, CA, Oct. 2006, IEEE Processing.

Szymas, J., Wolf, G., Papierz, W., Jarosz, B. & Weinstein, R. S. (2001). Online Internet-based robotic telepathology in the diagnosis of neuro-oncology cases: a teleneuropathology feasibility study. *Hum Pathol.* Vol. 32(12), pp. 1304-1308

Takaoka A., Yoshida K., Mori H., Hayashi S., Young S. J. & Ellisman M. H. (2000). International telemicroscopy with a 3 MV ultrahigh voltage electron microscope. *Ultramicroscopy*, Vol. 83(1-2), pp. 93-101

Wakida, N. M., Lee, C. S., Botvinick, E. L., Shi, L. Z., Dvornikov, A. & Berns, M. W. (2006). Laser Nanosurgery of Single Microtubules Reveals Time and Location Dependent Depolymerization Rates. *J. Biomed Opt*, Vol. 12(2)

Yamada A., Hirahara O., Tsuchida T., Sugano N., Date M. (2003). A practical method for the remote control of the scanning electron microscope. *J Electron Microsc.* Vol. 52(2), pp. 101-109.

Yeom, S., Javidi, B. (2006). Automatic identification of biological microorganisms using three-dimensional complex morphology. *J Biomed Opt.* Vol. 11(2), 024017

Youngblom J. H., Youngblom J. J., Wilkinson J. (2001). TelePresence Confocal Laser Scanning Microscopy. *Microsc Microanal*, Vol. 7(3), pp.241-248

Medical Robotics

Edited by Vanja Bozovic

The first generation of surgical robots are already being installed in a number of operating rooms around the world. Robotics is being introduced to medicine because it allows for unprecedented control and precision of surgical instruments in minimally invasive procedures. So far, robots have been used to position an endoscope, perform gallbladder surgery and correct gastroesophogeal reflux and heartburn. The ultimate goal of the robotic surgery field is to design a robot that can be used to perform closed-chest, beating-heart surgery. The use of robotics in surgery will expand over the next decades without any doubt. Minimally Invasive Surgery (MIS) is a revolutionary approach in surgery. In MIS, the operation is performed with instruments and viewing equipment inserted into the body through small incisions created by the surgeon, in contrast to open surgery with large incisions. This minimizes surgical trauma and damage to healthy tissue, resulting in shorter patient recovery time. The aim of this book is to provide an overview of the state-of-art, to present new ideas, original results and practical experiences in this expanding area. Nevertheless, many chapters in the book concern advanced research on this growing area. The book provides critical analysis of clinical trials, assessment of the benefits and risks of the application of these technologies. This book is certainly a small sample of the research activity on Medical Robotics going on around the globe as you read it, but it surely covers a good deal of what has been done in the field recently, and as such it works as a valuable source for researchers interested in the involved subjects, whether they are currently "medical roboticists" or not.

How to reference

In order to correctly reference this scholarly work, feel free to copy and paste the following:

INTECH
open science | open minds

51000 Rijeka, Croatia
Phone: +385 (51) 770 447
Fax: +385 (51) 686 166
www.intechopen.com

中国上海市延安西路65号上海国际贵都大饭店办公楼405单元
Phone: +86-21-62489820
Fax: +86-21-62489821